

Fabric transpositions in granite plutons - an insight from non-scaled analogue modelling

Zuzana Kratinová^{a, b}, Matěj Machek^a and Vladimír Kusbach^{c, d}

^a Institute of Geophysics AS CR, v.v.i, Boční II/1401, 14131, Prague 4, Czech Republic, mates@ig.cas.cz

^b Centro de Geofísica da Universidade de Lisboa/IDL, Campo Grande, Edifício C8, 1749 - 016 Lisboa - Portugal

^c Institute of Petrology and Structural Geology, Charles University, Prague, Czech Republic

^d Centre de Géochimie de la Surface, EOST, UMR 7516 Université Louis Pasteur, Strasbourg cedex, France

published in *Journal of the Geological Society of India* 75 (2010) 267-277

Investigations on a set of experimental models of highly viscous intrusions were carried out in order to study the internal strain pattern during vertical ascent and emplacement of granite intrusions. The strain pattern was determined by means of anisotropy of magnetic susceptibility (AMS) resulting from the orientation of magnetite particles in a liquid plaster medium. The modelled intrusions show distinct fabrics reflecting the flow of a rheologically complex, non-Newtonian material. During the vertical growth of the intrusion, constrictional vertical fabrics are transposed into flattening fabrics, and along with the development of low-intensity fabric domains are passively transported upwards. Vertical growth takes place along subvertical thrust shear zones that satisfactorily explain the discordant magmatic fabrics in granites along intrusion sides. The resulting complex fabric patterns suggest that the vertical movement of material in ascending intrusions is accommodated by various flow mechanisms operating simultaneously.

1 Introduction

Emplacement of granitic intrusions has been the subject of numerous experimental and theoretical studies (Pitcher, 1987; Weinberg and Podladchikov, 1994; Collins and Sawyer, 1996; Petford, 1996; Roman-Berdiel, 1999; Weinberg, 1999; Simakin and Talbot, 2001; Leitch and Weinberg, 2002). After the first experimental models were published by Grout (1945), an important progress resulted from using the centrifuge technique (Ramberg, 1981). Most of the models have improved our understanding of final intrusion shapes, some of them have included the role of multiple pulses and regional deformation (Dietl and Koyi, 2002) and have been designed to compare with natural examples (Dietl and Koyi, 2008).

The crucial information for the interpretation of magmatic processes associated with the emplacement of plutons is recorded in their internal fabrics (e.g. Castro, 1987; Ramsay, 1989; Fernandez and Laporte, 1991; Boullin et al., 1993; Bouchez, 1997; Paterson et al., 1998; Archanjo et al., 2002; Esmaeily et al., 2007). Therefore, an understanding of the formation of the internal fabrics during magma flow according to particular pluton geometries represents an important piece of information. Large-scale mapping of fabric patterns in granite plutons has become a commonly used structural method to characterize deformation, pluton evolution and to put forward a hypothesis of magma emplacement mechanism (Benn et al., 2001; Archanjo et al., 2008; Majumder and Mamtani, 2009; Raposo et al., 2009). The application of anisotropy of the magnetic susceptibility (AMS; Tarling and Hrouda, 1993) on magmatic regions (Bouchez, 1997) has significantly increased and is nowadays used as a major structural method to investigate the internal fabrics of magmatic rocks (e.g. Bouchez et al., 1990; Benn et al., 1998). Nevertheless, our understanding of pluton construction is biased by the access to a given erosion level. Therefore, interpretations of 3-D shape and vertical extent of a pluton based on 2-D sections are largely speculative.

Research in experimental modelling of intrusions led to improved understanding of the dynamics of magma emplacement (Bonini et al., 2001), but efforts are still required to understand the internal strain and the associated fabric development in plutons during emplacement. Until now, analogue models devoted to internal fabric investigation used materials of Newtonian rheologies (Schwerdtner and Troeng, 1978; Buisson and Merle, 2002), hence oversimplifying the realistic rheological properties of magmas and their changes during magma flow (cf. Bagdassarov and Pinkerton, 2004).

In this paper, flow structures of magma intrusion are satisfactorily modelled using "Plaster of Paris" (Kratinová et al., 2006). Through the addition of magnetic particles, the internal fabric patterns reflecting the flow and deformation are quantified by means of AMS. In order to investigate significant fabric patterns that are produced during magmatic intrusions, we performed several experiments at different intrusion conditions and using apparatuses having different injection geometry. The AMS was provided by the addition of fine-grained pure magnetite. We will demonstrate that the reproducible structures modelled have significance for fabric interpretation in granite bodies.

2 Experimental set-up

A set of non-scaled experiments of viscous intrusion were designed to investigate the evolution of internal fabric patterns during vertical ascent and emplacement of magma. The internal strain patterns were constrained by means of AMS that resulted from the orientation of magnetite particles in the liquid plaster medium and by the patterns of the contrast-staining of liquid plaster. Experiments were carried out using three apparatuses with different intrusion parameters and injection architectures that helped to find common and significant structural features which may be potentially important for fabric interpretation in magmatic intrusions.

2.1 Properties of the analogue material

The intrusive material modelled with liquid plaster is a suspension of fibrous particles dispersed in water. The plaster is characterized by a shear-thinning rheology and thixotropic properties (Závada et al., 2008). This behaviour is similar to dispersions

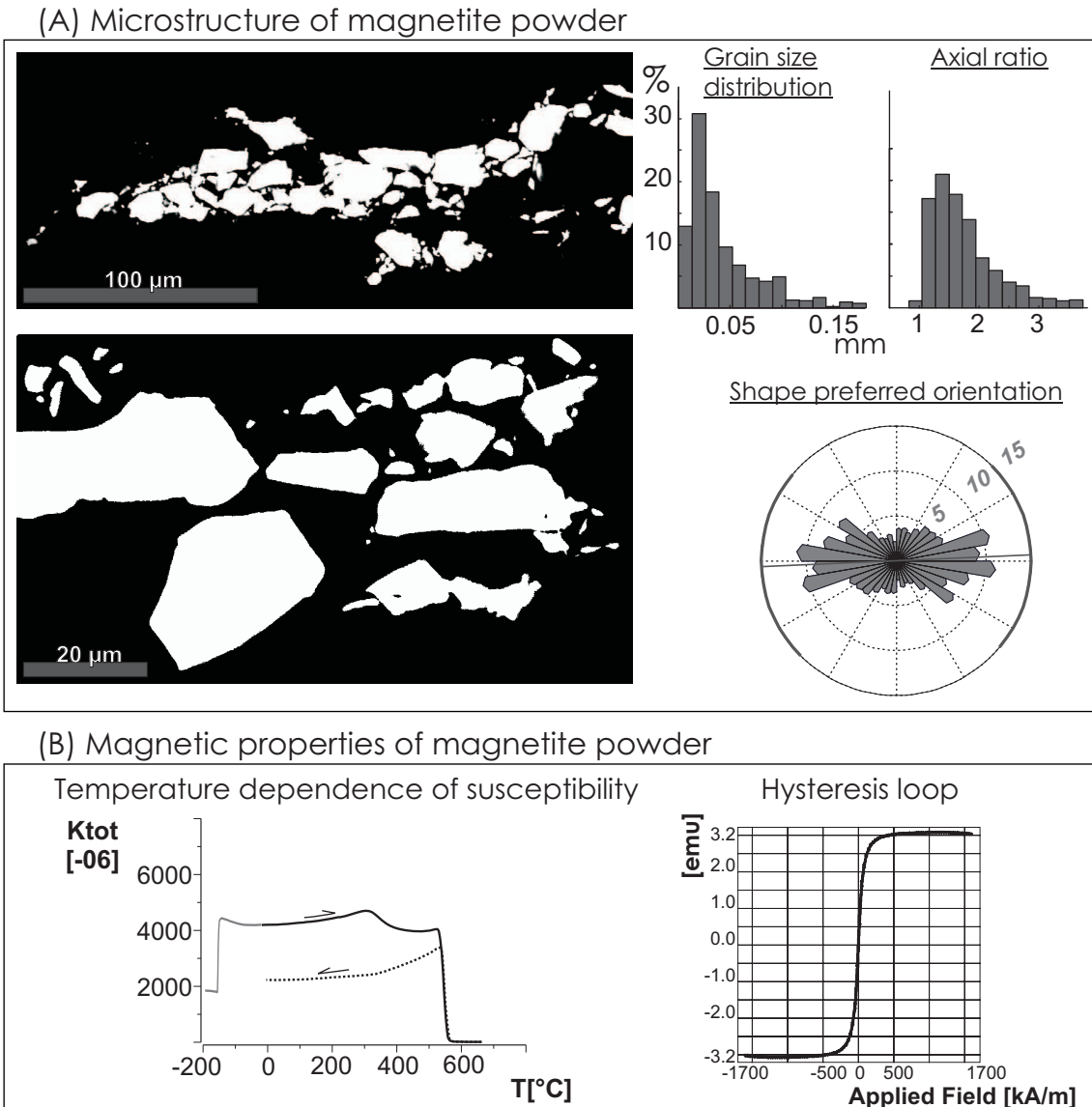


Fig. 1. Properties of magnetite particles used as a tracer for the AMS fabric. (a) BSE images of magnetite particles oriented in magnetic field and quantitative microstructural analyses. (b) Properties of the magnetite powder: temperature-susceptibility dependence and hysteresis curve. The temperature-susceptibility data were measured using the CS-3 and CS-L Cryostat Apparatus attached to the KLY-4S Kappabridge (Hrouda, 1994; Jelínek and Pokorný, 1997). The hysteresis parameters were measured on ADE EV9 VSM in Geophysical Institute, Prague.

having 'gel' structure defined by a network of interacting particles, in which the disruption of the network (so-called 'sol') causes a drastic viscosity drop. In granitic magmas, such behaviour is provided by long chains of molecules in melt and by already crystallized minerals, such as feldspars. In our plaster, the size of particles in suspension ranges from 0.18 μm to 283 μm, with a median value $D_{50} = 7.20 \mu\text{m}$ and a mean value at 39.4 μm. Since a retarding powder (of composition unspecified by producer) was added to delay the solidification reaction all experiments were performed without any significant rheological change (see Závada et al., 2008). In order to track the material motion, individual plaster layers were colored before the experimental runs. The material to be intruded by the plaster and forming the surrounding host-rock is a

fine-grained (0.017 mm), almost pure quartz sand (Kratinová et al., 2006).

The properties of magnetite grains are given in Fig. 1a (for details see Kratinová et al., 2006; Závada et al., 2008). In order to determine the magnetic behaviour of the magnetite powder used, we have analyzed bulk susceptibility variations with temperature (from 25°C to 700°C and -195°C to 0°C) and hysteresis parameters. The temperature vs. magnetic susceptibility data of this material indicates that the grains are pure magnetite (Fig. 1b). The possible “inverse” AMS fabric (Rochette et al., 1999) due to very fine-grains is excluded by the multi-domain nature of the magnetite powder (Dunlop, 2002) as shown in Fig. 1b. To characterize the magnetite behaviour we have conducted a detailed grain size and shape analysis using the PolyLX Matlab toolbox (Fig. 1a; Lexa et al., 2005). The sizes of particles of magnetite have a lognormal size distribution with 70 % of grains in between 2 µm and 50 µm in diameter and a mean Ferret diameter of 44 µm. Their axial ratio ranges from 1.3 to 2 for 70 % of the grains with the mean axial ratio being 1.83. The magnetite grain shape suggests their easy orientation parallel to flow of plaster during evolution of the model. The very fine-grained magnetite used in experiments was homogeneously mixed with the plaster and does not show any tendency to segregate due to density differences.

2.2 Model design

In the three different apparatuses (Fig. 2) that were used to model granite intrusions, coloured plaster had to intrude an overlying sand-bed through cylindrical channel resulting in an axi-symmetric model. The first apparatus (Fig. 2a) is a cube-shaped Perspex container mounted on the base of a manual press (see Kratinová et al., 2006). The viscous material, pushed by the surface affected by vertical force, intrudes into the sand-bed through a circular orifice of 10 cm in diameter. With this apparatus the intrusion growth is accompanied by the addition of sand from the top. The second apparatus (Fig. 2b), driven by hydraulic press (Závada et al., 2008), works on a similar principle but the plaster intrudes a fixed height of overlying sand. The third apparatus (Fig. 2c) is a large sandbox having a central injection system formed by a horizontal cylinder ending into a conduit, 5 cm in diameter, attached at the base of the sand box. In this set-up the coloured plaster pushed by the step-motor-driven piston intrudes into a constant height of the sand column. In all experiments no other external forces were applied and therefore modelled shapes and internal fabrics are results of vertical forces.

Five experiments of intrusive bodies are presented (Fig. 3). Models were conducted using dry plaster powder homogeneously mixed with 1wt % of retarding agent and 0.1 vol % of magnetite powder. A constant plaster/water mixing ratio of 2.2 was maintained during the experiments. Plaster preparation, homogenization and colouring are described in Kratinová et al. (2006). The first two experiments (A and B; Fig. 3), performed using the manual apparatus, represent two different growth stages of steep cylindrical intrusion reached at similar experimental conditions. During ascent of the intrusion that lasted 15 minutes, the sand was simultaneously deposited from the top giving constant weight of overburden. The second two experiments (C and D; Fig. 3) used the hydraulic press, lasted ~ 20 seconds and intruded a sand layer 50 cm thick. Experiment D was constrained by a planar inhomogeneity, made of a plastic thin foil preventing lateral expansion of material. The plaster introduced into the sandbox through a rectangular section (35 cm x 5 cm) resulting in a sheet-like intrusion. In the last experiment (E; Fig. 3) performed with the third apparatus, the viscous material intruded a

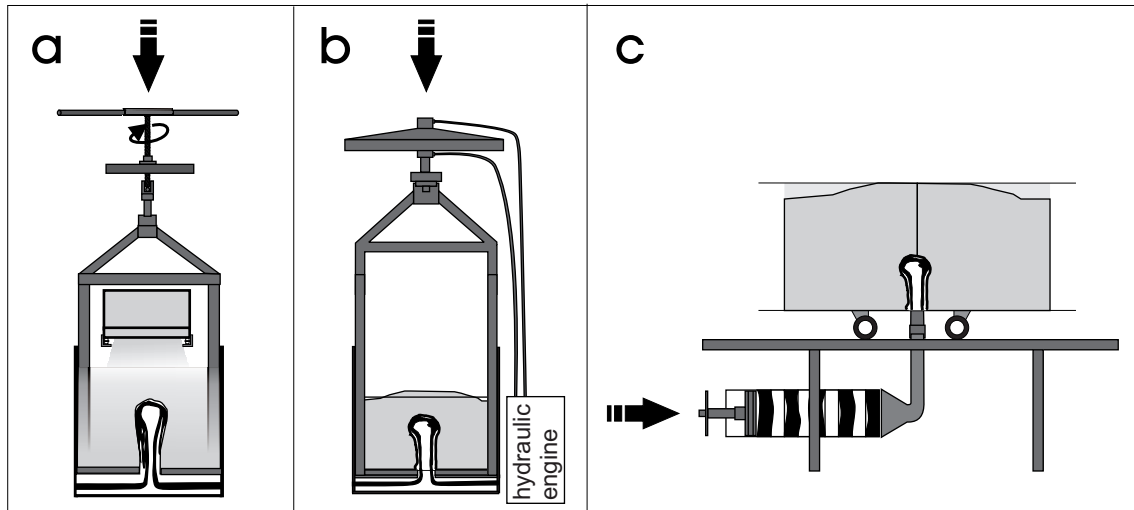


Fig. 2. Schematic illustration of analogue modelling apparatus. (a) Manual press apparatus (after Kratinová et al., 2006). Sand is deposited from the top during the experiment to keep a constant overburden. (b) Hydraulic press apparatus (after Závada et al., 2008). The material intrudes into the sand column of constant thickness. (c) Deformation sandbox. The arrow shows the direction of the applied external force that pushes the material into a sand column of constant thickness. The liquid plaster is coloured and the layers of black and white colour alternate either in horizontal (a, b) or in vertical (c) arrangement.

sand layer 50 cm thick in 10 minutes. The main differences in the experimental set-ups were therefore: duration of intrusion, sand layer thickness and size of intrusion.

2.3 Sampling and measurement

Once solidified, the models were cut along the XY vertical plane; X represents the orientation of the vertical axis of the model and Y being the left – right horizontal direction with respect to the frontal view of the model apparatus (Fig. 3). The section was drilled following a regular grid, the core diameter being 1 cm and core height 8 mm. The AMS of the cores was measured with the KLY-4S Kappabridge (Jelínek and Pokorný, 1997) and data were statistically evaluated using the ANISOFT software package (Jelínek, 1978; Hrouda et al., 1990). The eccentricity and shape of the AMS ellipsoid were characterized by the following parameters: $P = k_1/k_3$; $T = (2\ln k_2 - \ln k_1 - \ln k_3) / (\ln k_1 - \ln k_3)$; where $k_1 \geq k_2 \geq k_3$ are the principal susceptibilities (Nagata, 1961; Jelínek, 1981). The parameter P (degree of AMS) represents the intensity of the preferred orientation of magnetite, and T defines the symmetry of the AMS ellipsoid (the AMS ellipsoid is oblate for $0 < T < +1$ and prolate for $-1 < T < 0$). The orientations of magnetic foliation poles and magnetic lineations are presented in lower hemisphere equal-area projection.

3 Structural features of the models

In order to characterize the fabric pattern, we have compared the AMS with the spatial distribution and geometrical character of coloured layers. At their initial stages, the growth is quasi - axisymmetrical showing progressive inflation symmetrically along the vertical axes. Growth becomes asymmetric at later experiment stage when a lobate

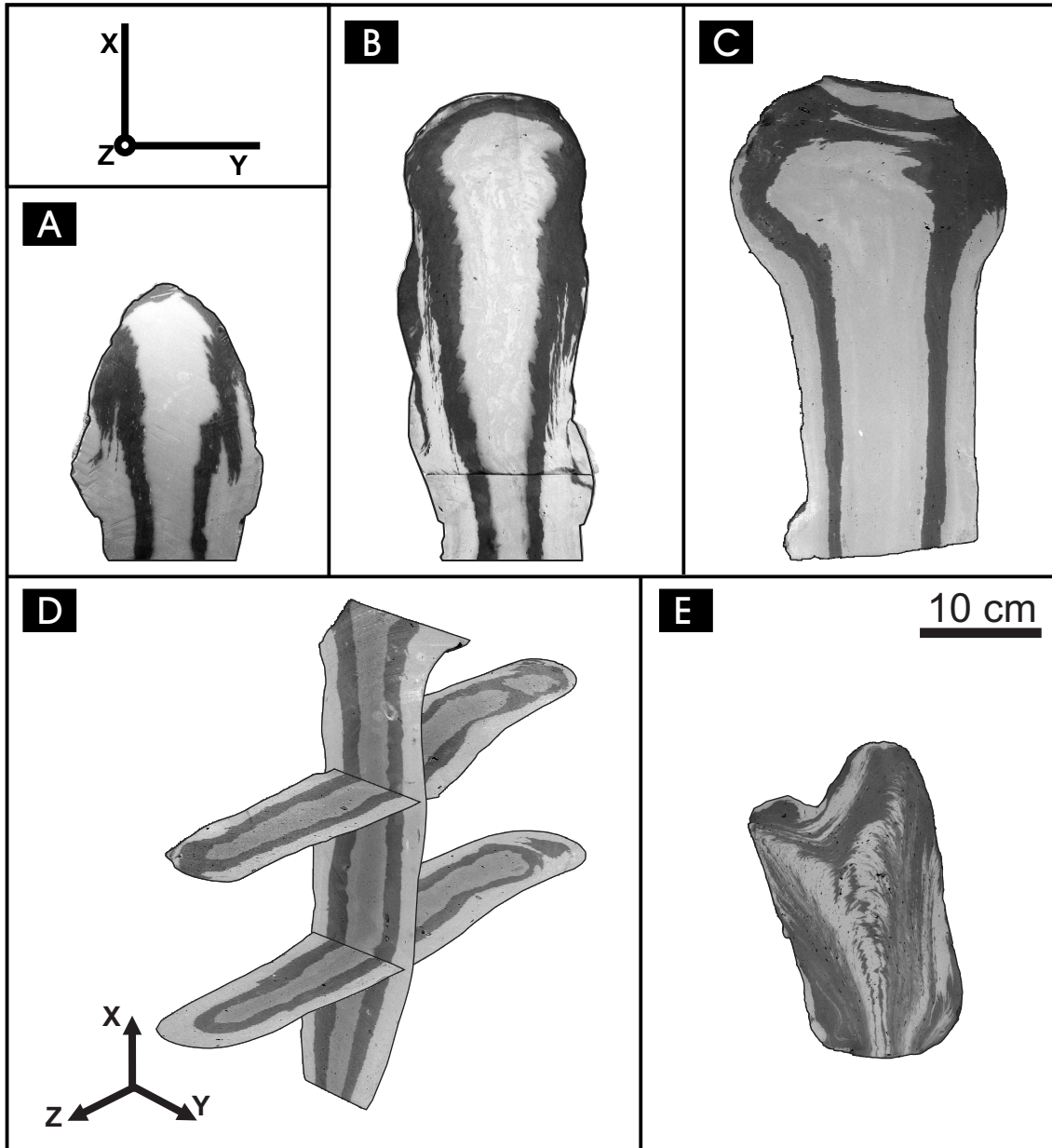


Fig. 3. Photographs of final intrusions obtained from individual experiments (A-E)

structure forms due to preferential growth in one direction (model E). The internal flow is characterized by vertical displacement and lateral inflation. In the experiment D, the lateral expansion was limited by the walls of plastic sheet which constrained the emplacement space. The plaster intrusions rising through the sand overburden are manifested on the surface by the development of a fracture system. The sand layer is affected by the radial cracking and faulting above the most concave part. The deformation of loose sand comprises both, the predominant downward transport and localization of deformation in small-scale synkinematic faults. These fractures nucleate in the centre above the rising intrusion and propagate radially sidewise.

3.1 Intrusive flow fabrics

The plaster to be injected was coloured in three layers (white-black-white) (in models A to D) or in alternating volumes (model E) in order to visualize the transport of material and its kinematics (Fig. 3). Although the experiments were conducted under different conditions, the final models result in roughly similar patterns. The first model (Fig. 3; A) simulates the initial stage of an intrusion (26 cm in height) during which a continuous inflation forms a stocky dome-like body. The innermost white layer is marked by symmetrical black stripes which are folded in their upper parts. The second model (Fig. 3; B) shows an advanced cylindrical intrusion (42 cm in height). Examination along X reveals the progressive widening of the innermost white layer responsible for larger distance between the symmetrical black layers. The inner layer is fringed by symmetrical thick and inward pointing black stripes, from approximately one third of the column and, more pronounced towards the top of the intrusion. The symmetrical black stripes along the margins of intrusion are separated from the central part by small-scale shear zones. The third model (Fig. 3; C) also represents an advanced intrusion (40 cm in height) but formed at a higher growth rate. The XY section reveals the vertical character of the column highlighted by the black layers, which get significantly thicker from approximately two-thirds of the intrusion height. The vertical black layer becomes sub-horizontal in the top part. Transposition from vertical to horizontal is characterized by the thickening and buckling of the coloured layers. The fourth model (Fig. 3; D) (35 x 5 x 35 cm in size) simulates a sheet-like or tabular intrusion constrained by a heterogeneity in the crust represented by planar discontinuity (thin plastic foil) in this experiment. The coloured layers mark clearly the overall vertical structure, which broadens from the first third of its height. The fifth model (Fig. 3; E) (26 cm in height), represents a complex intrusion of slow-rate growth. This model shows an asymmetrical intrusion with two lobes and well-developed vertical shear zones along the lateral margins. In contrast, the centre of the intrusion reveals that very early buckling and curving of black layers took place.

3.2 Evolution of the AMS

The internal fabrics of all models were characterized by their AMS. From models A to E, Fig. 4 presents the directional and scalar values that are frequently used in such studies: magnetic foliation (plane perpendicular to k_3), the magnetic lineation (k_1), the shape (T) and symmetry (P) parameters. In all models, the lower part of the intrusion is characterized by vertical tube-like fabric patterns. In the central part of the models, the magnetic foliations and lineations abruptly change into the horizontal direction. In models A, B and C the fabric change occurs at a higher level than in models D and E. The walls of the intrusions are mainly characterized by imbricated to vertical fabrics.

The anisotropy degree (P) is given in the third column of the Fig. 4. At the base of the models, in the centre of the vertical channels relatively high P values ($P \sim 1.3$) are observed. This contrasts with the central parts of all the intrusions in which the relatively intense fabrics become low or even present the lowest values ($P \sim 1.1$). These low intensity domains develop in the middle of the columns, while their margins have much higher P values ($P \sim 1.25$). At the top of the intrusions, where the magnetic foliations are close to horizontal, an important intensification in fabric is observed, particularly in model C.

The shapes of the AMS ellipsoids (last column of the Fig. 4) are similar for the different models, although their intensities are variable. At the base of the models, the

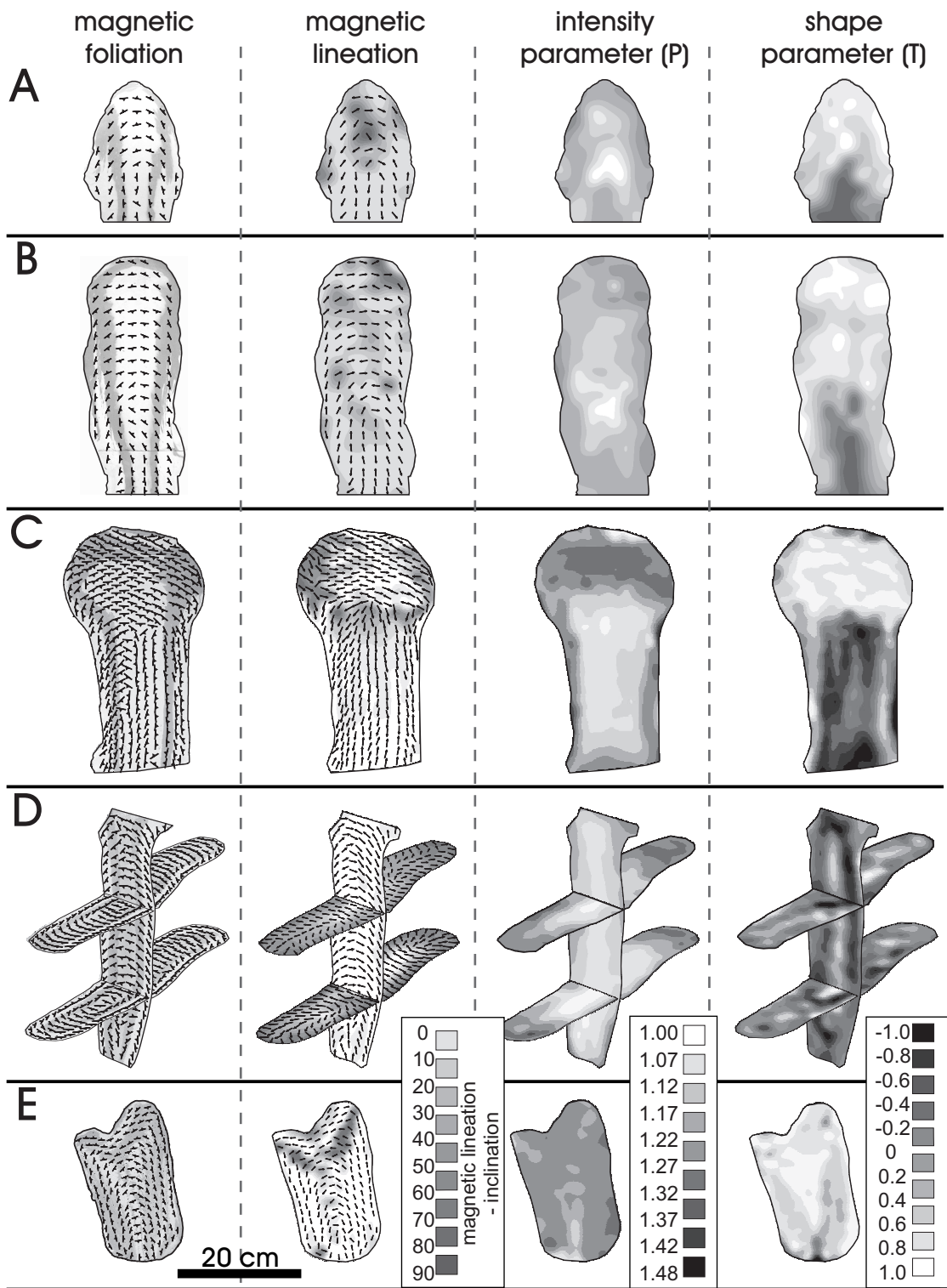


Fig. 4. Diagram representing AMS parameters viz. magnetic foliation, lineation, intensity (parameter P) and symmetry (parameter T) in different parts of each modelled intrusion. The background images for the magnetic foliation (first column) are the photographs of sections through models from figure 3. For the second column the background images represent the contoured magnetic lineation. The third and fourth columns respectively represent contoured degree of magnetic anisotropy (P) and shape parameter (T).

central part of each channel is characterized by highly prolate shapes ($T < 0$). By contrast, along the sides of the intrusions, plane strain ($T = 0$) to oblate shapes ($T > 0$) are observed. At places of models where the foliation becomes horizontal highly oblate shapes appear, with an exception of the model D.

3.3 Significant structural patterns

The two important features of our experimental models are the fabric transposition from vertical to subhorizontal towards the top of the models, and occurrence of subvertical shear zones crosscutting the previous horizontal and vertical fabrics along the borders of the models. In these experiments, fabric transposition occurs by destruction of the prolate subvertical AMS fabric (S1) and transposition into an oblate and subhorizontal fabric (S2) (Fig. 5). In models A and B, which have a slow growth rate, fabric transposition is located approximately in the half of the model height. In model C, which has a relatively fast growth rate, fabric transposition takes place in the upper third of the model. In the fast and tabular intrusion D and in the slow growing intrusion E the transposition occurs in the lower central part of the body. In all the models, the sharp changes in fabric orientation and shape, contrast with the wide domain of very low fabric intensity (Fig. 5).

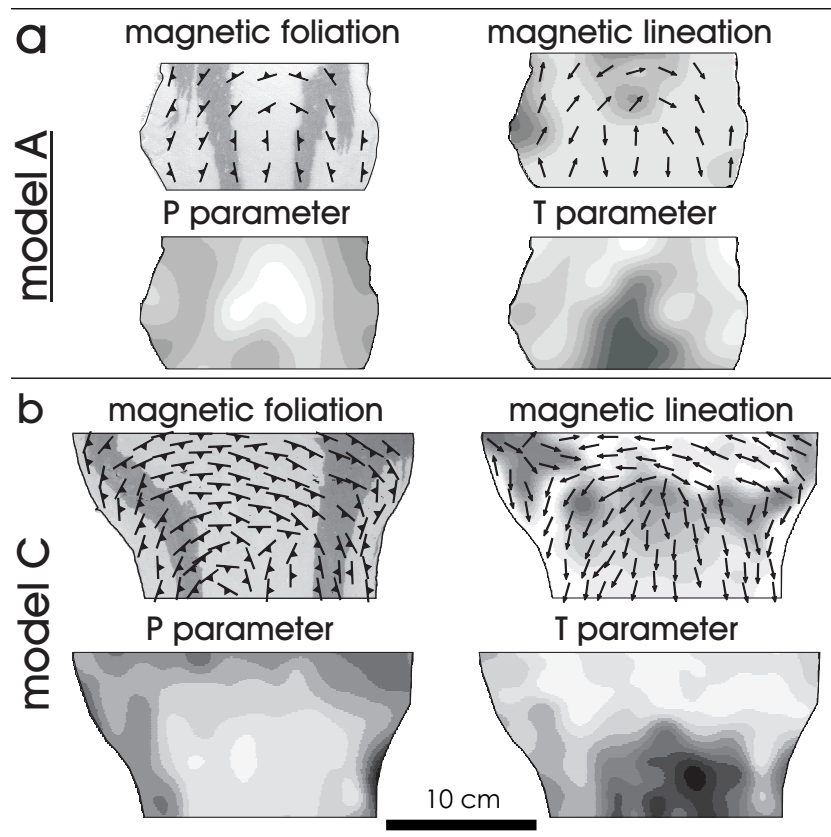


Fig. 5. Details of AMS fabric transposition domain in models A (a) and C (b). The constrictional vertical fabric is abruptly overprinted by the horizontal fabric. The domain of fabric transposition has the lowest magnetic intensity and is highly localized. Contours same as in Fig. 4.

The borders of all our models exhibit vertical shear zones (S3) reworking previous

horizontal (S2) and vertical (S1) fabric. In case of slowly growing models (A, B and E), the shear zones form parallel sets symmetrically disposed with respect to the intrusion axis. In the fast growing models (C and D), the shear zones are much narrower. In model B, which characterizes a more evolved intrusion stage than in model A, a larger number of well-developed shear zones are observed. Model E exhibits the best developed S3 shear zones (Fig. 6), which document a progressive rotation of S2 preserved in between shear zones, into vertical orientation towards model margins. The shear zones in all models exhibit a thrust character with respect to the vertical axis, which is well illustrated in the model E (Fig. 6). The magnetic fabric in the shear zone domains is characterized by medium intensities and mostly plain strain ellipsoid shape. The magnetic foliation is in these lateral parts of the model mostly parallel to S3 (rotated S2) and the lineations are vertical.

4 Discussion

4.1 Fabric interpretation

Although the magnetic fabrics and the coloured layering reveal a complex pattern, similar trends of fabric orientation and transposition are observed in all models. The lower parts of the intrusions reveal steep foliations (S1) arranged in a tube-like geometry with vertical lineations and highly constrictional shape fabrics. The constrictional fabrics reflect the convergent flow from the base towards the narrow channel and increasing strain rate. Towards the upper part of the intrusions, the material is homogeneously and progressively reworked by an increasing vertical pure-shear component that results in oblate imbricated subhorizontal foliations (S2). The transition zone between S1 and S2 fabrics is characterized by region of the lowest fabric strength. The detail of well developed transition zones in models A and C is given in Fig. 5. The material flowing through the entrance orifice is not in velocity equilibrium with the growing intrusion; the vertical constrictional flow decelerates, diverges and balances with the gravitational forces and transforms into horizontal spreading. However, the overall direction of plaster transport associated with intrusion growth remains vertical. The increasing weight of the overlying plaster plays an important role in the formation of the first fabric transposition in all models. In models A and B, this effect is reinforced by the increasing confining pressure at base of the intrusions due to sand deposition during the experiment. In contrast, in intrusions with a constant thickness of sand layer (models C and E) fabric transposition is controlled by the decreasing confining pressure at head of intrusion, allowing intrusion to expand laterally. Fabric transposition also takes place in the tabular model D, implying that this structural feature is not restricted only to intrusions of cylindrical shapes. Quantifying of the balance between plaster ascent and vertical load would require larger series of experiments and is not possible from the presented models.

The borders of the intrusions are the sites of shear strain localization allowing vertical growth of intrusion and upward transport of plaster through the transposition domain. Strain concentration leads to new sets of steep and parallel shear zones (S3) that develop between the actively growing inner part of the intrusion and the walls of the intrusion, and these show the thrust motion (Fig. 6). Such S3 shear zones overprint and rotate previous fabrics into subvertical orientations. The rate of growth and the growth stage seems to control the width of the shear zone, or the number of shear zones along the intrusion sides, as well as intensity of their offsets.

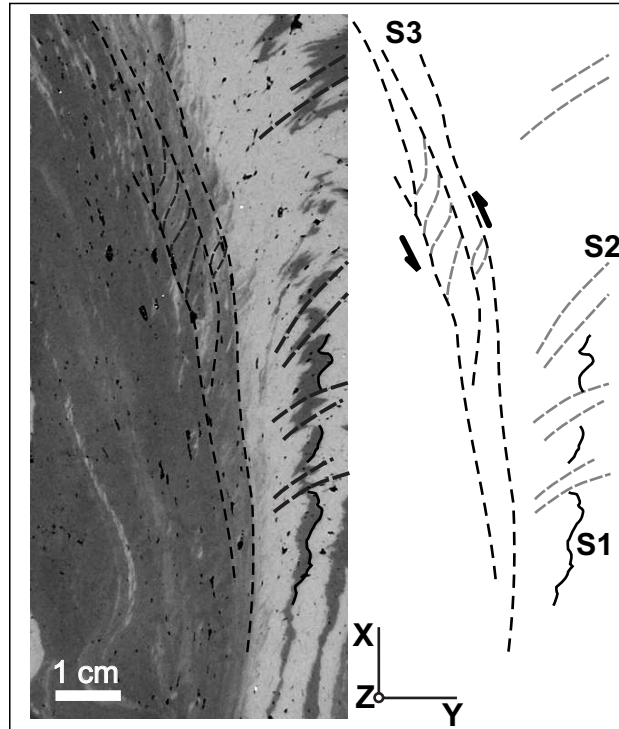


Fig. 6. Photograph taken from the experiment E. Detail of the shear zone domain showing well developed S3 structures with thrust motion, and fabric development from vertical (S1) through horizontal (S2) then to vertical (S3) fabric.

4.2 The role of strain-rate dependent rheology

Studies of the rheological properties of realistic magmas and lavas argue for complex non-Newtonian time-dependent behaviours associated with intrinsic structural changes (Bagdassarov and Pinkerton, 2004). In our experiments, the analogue material is temperature independent, but nevertheless exhibits a complex behaviour characterized by a strain-rate dependent rheology, thixotropy and the presence of yield strength. Departure of crystalline melts from Newtonian behaviour mostly comes from the development of crystal structures related to particle interactions. In terms of microstructures, the shear-thinning is related to viscosity decrease due to destruction of internal structures under increased shear stress and it is followed by a delayed restoration of the initial viscosity when the stress decreases (thixotropy). An important consequence of this behaviour relates to transitions from low stress conditions, where the crystal network inhibits flow movement and leads to the development of a yield strength, towards higher stress conditions in which network destruction and orientation of particles during shearing leads to an important decrease in effective viscosity. We consider that these properties of the plaster used in the experiments have rheological similarities with a crystallizing magma mush. Hence the plaster is a useful analogue of the latter. We suggest that our models show internal heterogeneous rheological behaviours, which determine partitioning into domains of distinct deformation and fabric patterns. It is likely that the moving material rising upwards has a plastic liquid-like behaviour, while the already emplaced material a solid-like behaviour. The rheological gradients related to fluctuations in effective viscosity imply that several flow mechanisms can operate simultaneously in the model during intrusion.

Three types of vertical transport of plaster are modelled in the presented intrusion experiments. In the central lower part of intrusions, the vertical transport is provided by the laminar vertical flow resulting in S1 fabric (Fig. 6). The S1 fabric is further overprinted by the horizontal oblate fabric S2 (Fig. 6), due to balance of vertical flow with gravitational forces. The intrusive material is passively transported to the upper level of intrusion supported by the ongoing flow force of intruding material. This vertical transport is accompanied by the horizontal spreading and widening of the intrusion. The vertical movement of the actively growing inner part leads to the shear strain concentration along the side walls of intrusions and to the development of subvertical shear zones (S3) associated with the thrust kinematics.

4.3 Relevance of modelled structures to granite plutons

Magmatic fabrics in granite plutons represent an important structural tool yielding information about magma ascent and emplacement or regional strain and many authors have discussed their significance in granitic rocks (e.g. Bouchez et al., 1990; Benn et al., 2001; Kratinová et al., 2007; Žák et al., 2008). These fabrics, usually interpreted in terms of internal magmatic processes, illustrate the complexity of flow in large magma chambers and represent processes, which cannot be easily constrained by field observations. A number of intrusions exhibit large fabric variations and even discordant magmatic fabrics (e.g. Schulmann, et al., 1997). In multiple intrusions, the contrasting fabrics at pluton scale can be interpreted as a result of multiple flows with different strain rates, while discordant fabrics in single intrusions require some other explanation. Such fabrics are interpreted in terms of superposition of solid-state and magmatic strains (Žák et al., 2005), subsolidus deformation of crystal-rich mush (Vernon et al., 2004) or switch of fabric orientation in transpressional shear zones (Parry et al., 1997). However, the erosion level of granite plutons does not usually provide information about their three-dimensional fabric architecture, thus limiting the interpretations about their flow and emplacement.

Our models reveal that complex fabric patterns develop during the vertical growth of intrusions due to the complex rheology of the intruding material. Based on our experiments, we believe that according to the shear-thinning rheology of silicate magmas, high-angle fabrics can potentially develop at a given structural level in a pluton, such as in nested heterogeneous plutons (Paterson and Vernon, 1995). We assume that rheological gradients explain the commonly observed abrupt changes in fabric intensity or orientation at the meter-scale. It is well-known that large magma chambers exhibit heterogeneous contents of feldspar phenocrysts which can be locally highly cumulated (Vernon and Paterson, 2008). The varying amounts of framework structure-bearing particles is probably the main factor favouring a highly localized flow with a low effective viscosity. Such mechanical instabilities are likely common structural phenomena in crystallizing magmas.

5 Conclusions

Several models were designed to investigate the fabric patterns during ascent and emplacement of highly viscous granite intrusions. Despite the necessary simplification of complexities of natural processes, we consider that our analogue experiments are relevant in terms of rheology and fabric geometry. The analogue material shows a complex non-Newtonian behaviour characterized by a strain-rate-dependent viscosity,

thixotropy and yield strength, properties usually described for crystal-bearing silica melts.

Two common fabric features are suggested to be significant for the interpretation of fabrics in natural plutons: (1) the rise of the intrusions associated with the transposition of the flow fabrics from vertical to horizontal, and (2) development of vertical shear zones along the intrusion sides. Our model suggests that during ascent several flow mechanisms may operate simultaneously, strengthening the fact that the rheological behaviour plays a key role in building the flow fabric in granites.

Acknowledgements

The authors are grateful to Jean-Luc Bouchez and Jean-Louis Vigneresse for their constructive reviews, which significantly helped to improve the manuscript, and to Manish A. Mamtani for his careful editorial work. Miroslav Roxer is gratefully acknowledged for his help with experiments and apparatus development. This work benefited from the financial support from GAAV No. KJB300120702 and from resources of the research intent to Geophysical Institute of the Academy of Sciences of the Czech Republic No. AV0Z30120515.

References

- Archanjo, C., Trindade, R., Bouchez, J.-L. and Ernesto, M. (2002) Granite fabrics and regional-scale strain partitioning in the Seridó belt (Borborema Province, NE Brazil). *Tectonics*, v. 21(1), pp. 1-13.
- Archanjo, C., Hollanda, M.H., Rodrigues, S., Neves, B. and Armstrong, R (2008) Fabrics of pre- and syntectonic granite plutons and chronology of shear zones in the Eastern Borborema Province, NE Brazil. *Jour. Struct. Geol.*, v. 30(3), pp. 310-326.
- Bagdassarov, N. and Pinkerton, H. (2004) Transient phenomena in vesicular lava flows based on laboratory experiments with analogue materials. *Jour. Volcanol. Geoth. Res*, v. 132, pp. 115-136.
- Benn, K., Ham, N. M., Pignotta, G. S. and Bleeker, W. (1998) Emplacement and deformation of granites during transpression: magnetic fabrics of the Archean Sparrow pluton, Slave Province, Canada. *Jour. Struct. Geol.*, v. 20(9/10), pp. 1247-1259.
- Benn, K., Paterson, S. R., Lund, S. P., Pignotta, G. S. and Kruse, S. (2001) Magmatic Fabrics in Batholiths as Markers of Regional Strains and Plate Kinematics: Example of the Cretaceous Mt. Stuart Batholith. *Phys. Earth Planet. In., Part A: Solid Earth and Geodesy (A)*, v. 26(4-5), pp. 343-354.
- Bonini, M., Sokoutis, D., Mulugeta, G., Boccaletti, M., Corti, G., Innocenti, F., Manetti, P. and Mazzarini, F. (2001) Dynamics of magma emplacement in centrifuge models of continental extension with implications for flank volcanism. *Tectonics*, v. 20(6), pp. 1053-1065.
- Bouchez, J.L. (1997) Granite is never isotropic: an introduction to AMS studies of granitic rocks. In: Bouchez, J.L., Hutton, D.W.H. and Stephens, W.E. (Eds.) *Granite: From Segregation of Melt to Emplacement Fabrics*, Kluwer Acad. Publ., Dordrecht, The Netherlands, pp. 95-112.

- Bouchez, J. L., Gleizes, G., Djouadi, T. and Rochette, P. (1990) Microstructure and magnetic susceptibility applied to emplacement kinematics of granites: the example of the Foix pluton (French Pyrenees). *Tectonophysics*, v. 184, pp. 157-171.
- Bouillin, J.P., Bouchez, J.L., Lespinasse, P. (1993) Granite emplacement in an extensional setting - an AMS study of the magmatic structures of Monte-Capanne (Elba, Italy). *Earth Planet. Sc. Lett.*, v. 118 (1-4), pp. 263-279.
- Buisson, C. and Merle, O. (2002) Experiments on internal strain in lava dome cross sections. *B. of Volcanol.*, v. 64(6), pp. 363-371.
- Castro, A. (1987) On granitoid emplacement and related structures - a review. *Geol. Rundsch.*, v. 76, pp. 101-124.
- Collins, W.J. and Sawyer, E.W. (1996) Pervasive granitoid magma transfer through the lower-middle crust during non-coaxial compressional deformation. *Jour. Metam. Geol.*, v.14, pp.565-579.
- Dietl, C. and Koyi, H. A. (2002) Emplacement of nested diapirs: Results of centrifuge modelling. *Jour. of the Virtual Explorer*, v. 6, pp. 81-88.
- Dietl, C. and Koyi, H. A. (2008) Formation of tabular plutons - results and implications of centrifuge modelling. *Jour. of Geosciences*, v. 53, 253-261.
- Dunlop, D. J. (2002) Theory and application of the Day plot (M-rs/M-s versus H-cr/H-c) 2. Application to data for rocks, sediments, and soils. *Jour. Geophys. Res.*, v. 107, B3.
- Esmaeily, D., Bouchez, J.L. and Siqueira, R. (2007) Magnetic fabrics and microstructures of the Jurassic Shah-Kuh granite pluton (Lut Block, Eastern Iran) and geodynamic inference. *Tectonophysics*, v. 439(1-4), pp. 149-170.
- Fernandez, A. and Laporte, D. (1991) Significance of low symmetry fabrics in magmatic rocks. *Jour. Struct. Geol.*, v. 13(3), pp. 337-347.
- Grout, F. F. (1945) Scale models of structures related to batholiths. *Am. J. Sci.*, v. 243A, pp. 260-284.
- Hrouda, F. (1994) A Technique for the Measurement of Thermal-Changes of Magnetic-Susceptibility of Weakly Magnetic Rocks by the Cs-2 Apparatus and Kly-2 Kappabridge. *Geophys. Jour. Int.*, v. 118(3), pp. 604-612.
- Hrouda, F., Jelinek, V. and Hruskova, L. (1990) A package of programs for statistical evaluation of magnetic data using IBM-PC computers. AGU 1990 fall meeting. *Eos, Transactions, American Geophysical Union*, v. 71(43), pp. 1289.
- Jelínek, V. (1978) Statistical processing of anisotropy of magnetic susceptibility measured on groups of specimens. *Stud. Geophys. Geod.*, v. 22, pp. 50-62.
- Jelínek, V. (1981) Characterization of magnetic fabric of rocks. *Tectonophysics*, v. 79, pp. 63-67.
- Jelínek, V. and Pokorný, J. (1997) Some new concepts in technology of transformer bridges for measuring susceptibility anisotropy of rocks. *Phys. Chem. Earth*, v. 22, pp. 179-181.
- Kratinová, Z., Závada, P., Hrouda, F. and Schulmann, K. (2006) Non-scaled analogue modelling of AMS development during viscous flow: A simulation on diapir-like structures. *Tectonophysics*, v. 418(1-2), pp. 51-61.
- Kratinová, Z., Schulmann, K., Edel, J. B., Ježek, J. and Schaltegger, U. (2007) Model of successive granite sheet emplacement in transtensional setting: Integrated microstructural and anisotropy of magnetic susceptibility study. *Tectonics*, v. 26, TC6003, doi:10.1029/2006TC002035

- Leitch, A.M. and Weinberg, R.F. (2002) Modelling granite migration by mesoscale pervasive flow. *Earth Planet. Sci. Lett.*, v. 200(1-2), pp.131-146.
- Lexa, O., Štípská, P., Schulmann, K., Baratoux, L., Kröner, A. (2005) Contrasting textural record of two distinct metamorphic events of similar P-T conditions and different durations. *Jour. Metam. Geol.*, v. 23(8), pp. 649-666.
- Majumder, S. and Mamtani, M. A. (2009) Magnetic fabric in the Malanjkhand Granite (Central India)-Implications for regional tectonics and Proterozoic Suturing of the Indian shield. *Phys. Earth Planet. In.*, v. 172(3-4), pp. 310-323.
- Nagata, T. (1961) *Rock Magnetism*, Maruzen, Tokyo.
- Parry, M., Štípská, P., Schulmann, K., Hrouda, F., Ježek, J. and Kroner, A. (1997) Tonalite sill emplacement at an oblique plate boundary: northeastern margin of the Bohemian Massif. *Tectonophysics*, v. 280, pp. 61-81.
- Paterson, S. R., Fowler, T. K., Schmidt, K. L., Yoshinobu, A. S., Yuan, E. S. and Miller, R. B. (1998) Interpreting magmatic fabric patterns in plutons. *Lithos*, v. 44, pp. 53-82.
- Paterson, S. R. and Vernon, R. H. (1995) Bursting the bubble of ballooning plutons: A return to nested diapirs emplaced by multiple processes. *GSA Bulletin*, v. 107(11), pp. 1356-1380.
- Petford, N. (1996) Dykes and diapirs? *T. Roy. Soc. Edin-Earth*, v. 87, pp. 105-114. Pitcher, W.S. (1979) Nature, ascent and emplacement of granitic magmas. *Jour. Geol. Soc.*, v. 136, pp. 627-662.
- Ramberg, H. (1981) *Gravity, deformation and the Earth's crust*. Academic Press, New York.
- Ramsay, J. G. (1989) Emplacement kinematics of a granite diapir; the Chindamora Batholith, Zimbabwe. *Jour. Struct. Geol.*, v. 11(1-2), pp. 191-209.
- Raposo, M. I. B., Carmo, M. and Gastal, P. (2009) Emplacement mechanism of the main granite pluton of the Lavras do Sul intrusive complex, South Brazil, determined by magnetic anisotropies. *Tectonophysics*, v. 466(1-2), pp.18-31.
- Román-Berdiel, T. (1999) Geometry of granite emplacement in the upper crust: contributions of analogue modelling. *Geol. Soc. Spec. Publ.*, v.168, p. 77-94.
- Rochette, P., Aubourg, C., Perrin, M. (1999) Is this magnetic fabric normal? A review and case studies in volcanic formations. *Tectonophysics*, v. 307(1-2), pp. 219-234.
- Simakin, A. and Talbot, C. (2001) Tectonic pumping of pervasive granitic melts. *Tectonophysics*, v. 332, pp. 387-402.
- Schulmann, K., Ježek, J. and Venera, Z. (1997) Perpendicular linear fabrics in granite: markers of combined simple shear and pure shear flows? In: Bouchez, J.L., Hutton, D.W.H. Stephens, W.E. (Eds.) *Granite: From Segregation of Melt to Emplacement Fabrics*, Kluwer Acad. Publ., Dordrecht, The Netherlands, pp. 159-76.
- Schwerdtner, W. M. and Troeng, B. (1978) Strain distribution within arcuate diapiric ridges of silicon putty. *Tectonophysics*, v. 50, pp. 13-28.
- Tarling, D. H. and Hrouda, F. (1993) *The Magnetic Anisotropy of Rocks*, Chapman and Hall, London.
- Vernon, R. H., Johnson, S. E. and Melis, E. A. (2004) Emplacement-related microstructures in the margin of a deformed pluton: the San Jose tonalite, Baja California, Mexico. *Jour. Struct. Geol.*, v. 26, pp.1867-1884.

- Vernon, R.H. and Paterson, S.R. (2008) *How late are K-feldspar megacrysts in granites?* *Lithos*, v. 104(1-4), pp. 327-336.
- Weinberg, R.F. (1999) *Mesoscale pervasive melt migration alternative to dyking.* *Lithos*, v. 46, pp. 393-410.
- Weinberg, R. F. and Podladchikov, Y. (1994) *Diapiric ascent of magmas through power law crust and mantle.* *Jour. Geophys. Res.*, v. 99(B5), pp. 9543-9559.
- Závada, P., Kratinová, Z., Kusbach, V. and Schulmann, K. (2008) *Internal fabric development in complex lava domes.* *Tectonophysics*, v. 466(1-2), pp. 101-113.
- Žák, J., Schulmann, K. and Hrouda, F. (2005) *Multiple magmatic fabrics in the Sazava pluton (Bohemian Massif, Czech Republic): a result of superposition of wrench-dominated regional transpression on final emplacement.* *Jour. Struct. Geol.*, v. 27, pp. 805-22.
- Žák, J., Verner, K. and Týcová, P. (2008) *Multiple magmatic fabrics in plutons: an overlooked tool for exploring interactions between magmatic processes and regional deformation?* *Geol. Mag.*, v. 145(4), pp. 537-551.